applied sciences

MDPI

Communication

Noise Differentiation and Atom Number Measurement in Optical Lattice Clocks by Analyzing Clock Stabilities with Various Parameters

Guodong Zhao [1,2], Feng Guo [1], Xiaotong Lu [1,*] and Hong Chang [1,2,*]

[1] Key Laboratory of Time Reference and Applications, National Time Service Center, Chinese Academy of Sciences, Xi'an 710600, China; zhaoguodong@ntsc.ac.cn (G.Z.); guofeng@ntsc.ac.cn (F.G.)
[2] School of Astronomy and Space Science, University of Chinese Academy of Sciences, Beijing 100049, China
* Correspondence: luxiaotong@ntsc.ac.cn (X.L.); changhong@ntsc.ac.cn (H.C.); Tel.: +86-029-83890852 (X.L.)

Abstract: We propose a method that enables the precise determination of the number of atoms in a Dick-noise-free optical lattice clock, by effectively addressing quantum projection noise. Our approach relies on conducting stability measurements at three distinct parameter sets, allowing us to differentiate between quantum projection noise, photon shot noise, and technical noise. Importantly, it enables accurate extraction of the atom number, even in the presence of photon shot noise and technical noise. We utilize numerical simulations to validate our approach, optimize the modulation parameters for minimal uncertainty, and investigate the impact of atom number fluctuations on the determinacy of our results. The numerical results show the validity of our method and demonstrate an estimated uncertainty in the atom number that is below 4% with 6.7 h measurement, provided that the standard deviation of atom number fluctuation is kept below 0.14 times the average atom number.

Keywords: atom number measurement; noise analysis; clock stability; optical clocks

check for updates

Citation: Zhao, G.; Guo, F.; Lu, X.; Chang, H. Noise Differentiation and Atom Number Measurement in Optical Lattice Clocks by Analyzing Clock Stabilities with Various Parameters. *Appl. Sci.* **2024**, *14*, 1758. https://doi.org/10.3390/app14051758

Academic Editor: David Petrosyan

Received: 18 January 2024
Revised: 16 February 2024
Accepted: 20 February 2024
Published: 21 February 2024

1. Introduction

Ultra-cold atoms confined within an optical lattice have played a pivotal role in the development of modern atomic clocks [1–3], the advancement of quantum techniques [4–8], and the exploration of fundamental physics [9–12]. Accurate determination of the atom number in the lattice is crucial to fully harness the potential of these applications. For instance, precise knowledge of the atom number is essential for studying many-body interactions [13,14], thereby reducing systematic uncertainties in optical lattice clocks (OLCs) [1–4].

Commonly employed methods for atom number measurement include fluorescence detection and absorption imaging [15–17]. However, the fluorescence detection method is typically limited by uncertainties arising from the effective solid angle and probe light intensity, resulting in a measurement uncertainty greater than 15% [15]. On the other hand, the absorption imaging technique offers a lower measurement uncertainty below 10%, relying on knowledge of the atomic sample shape and technical noise levels [16]. Recently, advancements in synchronized frequency comparison based on in situ measurements have effectively canceled out interrogation laser noise, improving measurement stability [18,19]. The comparison stability is constrained by atomic detection noises, including quantum projection noise (QPN), photon shot noise, and technical noise [20,21]. This progress has spurred the development of a new method to measure the atom number based on QPN. The previous method of measuring atom numbers from atomic detection noise required the neglect of technical noise [22]. This prerequisite prevented the utilization of atom number measurement based on the QPN.

In this paper, we present a method to distinguish the QPN noise, photon shot noise, and technical noise in a Dick-noise-free OLC [18,19,23–25]. By conducting three separate

stability measurements with modulations of the atom number (N_0) or the photon count (γ_0) detected per atom by the photoelectric detector, it becomes possible to extract the contributions of each noise responsible for clock stability. This method allows us to accurately determine the value of N_0 by differentiating QPN from other sources of noise. To further enhance precision, we use numerical simulations to investigate how modulation parameters influence the estimated uncertainty of N_0 and how measurement precision evolves as N_0 increases.

2. Methods

2.1. Theory

Assuming a transition probability of 0.5 and disregarding the detection laser noise, which is typically much less significant than other factors in an OLC [21], the clock stability σ_a at τ = 1 can be represented by [23,26]

$$\sigma_a^2 = \sigma_{QPN}^2 + \sigma_{Shot}^2 + \sigma_{Det}^2. \tag{1}$$

In Equation (1), $\sigma_{QPN}^2 = T_0/4S_0^2N_0$ corresponds to the variance contributed by the QPN, with T_0 representing the clock cycle time, and $S_0 = 0.6\pi \times T_p$ denoting the frequency-sensitive slope of the spectrum at half-height point, where T_p is the interrogation time for the clock transition in each clock cycle. $\sigma_{Shot}^2 = T_0/4S_0^2N_0\gamma_0$ refers to the variance originating from the photon shot noise, while $\sigma_{Det}^2 = T_0\delta_N^2/2S_0^2N_0^2$ represents the contribution of the technical noise. Here, δ_N stands for the electronic detection noise, including the contribution of the amplifier, digitizer, dark current noise, and so on. As the three types of noise exhibit distinct dependencies on N_0 and γ_0; it becomes possible to differentiate them effectively by modulating N_0 and γ_0.

By controlling the detection laser intensity or its duration (T_{det}), γ_0 can be manipulated. Specifically, by adjusting T_{det} to T_{det}/α while keeping other parameters constant as defined in Equation (1), the value of γ_0 will change to γ_0/α. Consequently, the overall clock stability can be represented as

$$\sigma_b^2 = \sigma_{QPN}^2 + \alpha\sigma_{Shot}^2 + \sigma_{Det}^2. \tag{2}$$

In the same manner, by changing N_0 to N_0/β, we can separate the technical noise from other noises, and the overall clock stability is denoted by

$$\sigma_c^2 = \beta(\sigma_{QPN}^2 + \sigma_{Shot}^2) + \beta^2\sigma_{Det}^2. \tag{3}$$

Combining Equations (1)–(3), the contributions of different noise sources can be determined by solving

$$\begin{bmatrix} 1 & 1 & 1 \\ 1 & \alpha & 1 \\ \beta & \beta & \beta^2 \end{bmatrix} \begin{bmatrix} \sigma_{QPN}^2 \\ \sigma_{Shot}^2 \\ \sigma_{Det}^2 \end{bmatrix} = \begin{bmatrix} \sigma_a^2 \\ \sigma_b^2 \\ \sigma_c^2 \end{bmatrix}. \tag{4}$$

Once the value of σ_{QPN} is obtained using Equation (4), it becomes possible to determine the absolute atom number in an OLC.

2.2. Numerical Simulation Method

To validate our approach and identify the optimal modulation parameters (α and β) for minimizing the estimated uncertainty, we employ numerical simulations. The flow chart of this simulation is shown in Figure 1, which involves three main steps. In step 1, we set the values of T_p, T_0, N_0, γ_0, δ_N, α, and β, and calculate S_0, σ_a, σ_b, and σ_c. The noise-induced frequency fluctuation is represented by the discrete normal random numbers with the standard deviation of σ_a for case 1, σ_b for case 2, and σ_c for case 3. In step 2, the clock comparison process between two clocks is executed with a simulated time of approximately 2.2 h for each case. The total simulated time is obtained by multiplying the total clock cycle number by $3T_0$, where the reason of the use of $3T_0$ is that three measurements are required

in real-world scenarios to determine the values of σ_a, σ_b, and σ_c. In this work, the Dick effect is cancelled by setting the clock laser noise to be zero [27]. The cancellation of the Dick effect can be realized in experiment by synchronous frequency comparison between two clocks [23,28], or by using the in situ imaging technique to compare two regions of cold ensembles in a clock [18,19,22,25]. Regarding the simulation aspect of the in-loop clock operation, the excitation fractions at half-height points are determined by adjusting the center frequency of the Rabi spectrum by $\pm 0.4/T_p$. Subsequently, the corresponding generated discrete normal random numbers from step 1 are added to the determined excitation fraction, and the frequency corrections of each clock are calculated. These corrections are then utilized to update the center frequency of the Rabi spectrum. In step 3, upon completion of all clock cycles, the comparison stability is derived by computing the Allan variance of the frequency difference between the two clocks. It is worth noting that the Allan variance of a single clock should be divided by 2 [28]. Subsequently, the parameters of σ_{QPN}, σ_{Shot}, and σ_{Det} can be determined and the value of N_0 is determined by $T_0/4S_0^2\sigma_{QPN}^2$.

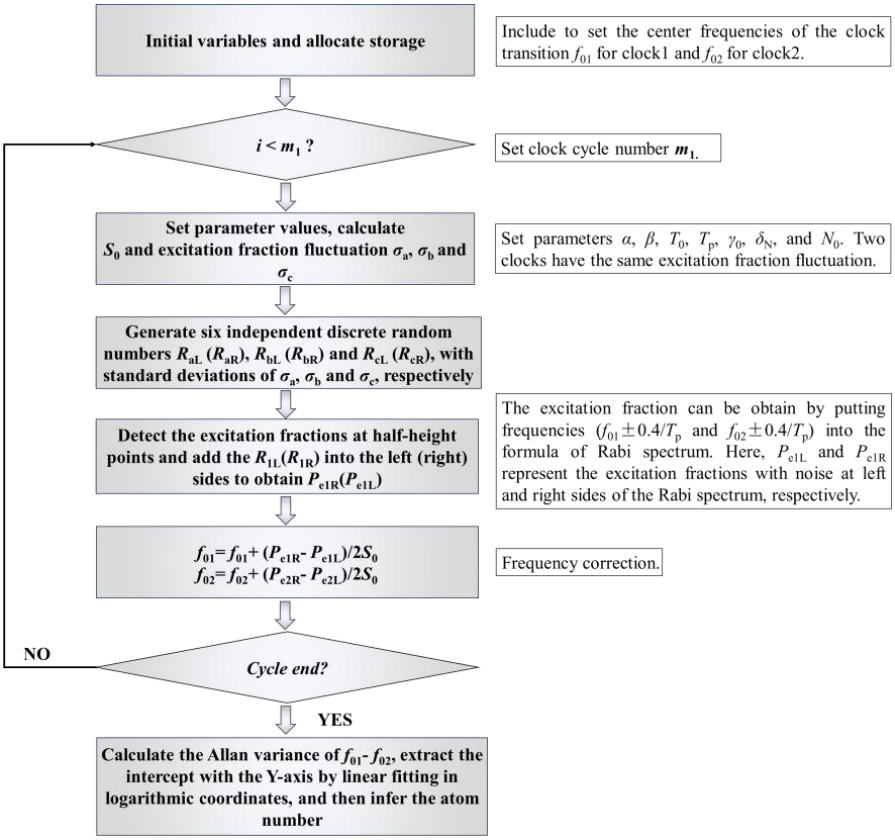

Figure 1. The flow chart of the numerical simulation.

In this work, we maintain T_0 at 1 s and utilize Rabi detection with a fixed interrogation time of T_p = 0.1 s, which can be easily implemented in the experiment. It is important to note that the specific choice of T_p has minimal impact on the numerical results obtained. The collision between atoms influences the atomic-density-dependent S_0 [13,14]. However, in our simulation, where T_p equals 0.1 s and the maximum atom number is lower than 6000, the system operates in the weak interaction region. Consequently, the variation in S_0 can be reasonably disregarded as the atom number changes [13,14]. Nevertheless, if the collision effects become prominent in a regime characterized by high density and strong interactions, the value of S_0 will be reduced due to density broadening. This reduction in S_0 indicates a higher level of instability for the clock.

3. Results and Discussion

To verify the accuracy of our numerical calculation code, we compare the stabilities obtained from numerical simulations at three sets of parameters to the theoretical results shown in Figure 2. The parameters used for this comparison are T_0 = 1 s, N_0 = 500, γ_0 = 1, δ_N = 3 [23], α = 0.2, β = 0.1. The excellent agreement observed in Figure 2 between the numerical and theoretical results confirms the correctness of our code and the validity of our method.

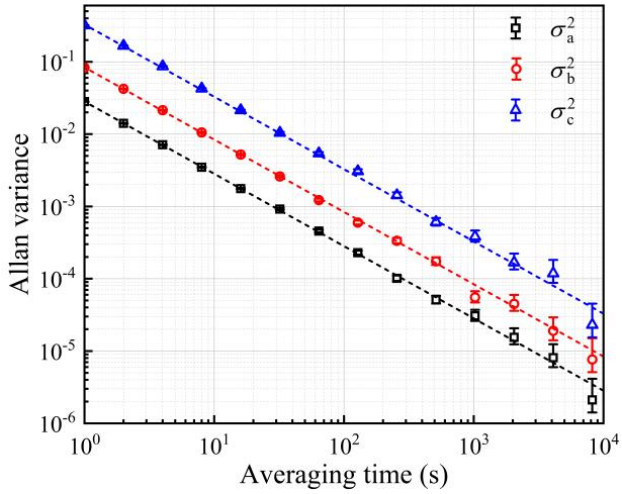

Figure 2. Comparisons of numerical and theoretical results of stabilities. The Allan variances of frequency fluctuations at three-group parameters. The points represent the numerical results and dashed lines indicate the corresponding theoretical results. All error bars represent the 1σ standard error.

We investigate the influence of α and β on the estimated uncertainty of N_0 by studying the standard deviation of 50 independent simulations at different combinations of α and β, as shown in Figure 3a for N_0 = 500 and Figure 3b for N_0 = 2000. The white regions in both figures indicate errors larger than 500 for Figure 3a and 2000 for Figure 3b, which occurs when α or β approaches 1. In such cases, the modulation amplitudes of the parameters become close to zero, indicating that the different noises cannot be distinguished. Similar uncertainty distributions are observed for both cases. The smallest uncertainty is achieved at α = 5.71 and β = 0.1 for N_0 = 500, and α = 3.84 and β = 0.27 for N_0 = 2000.

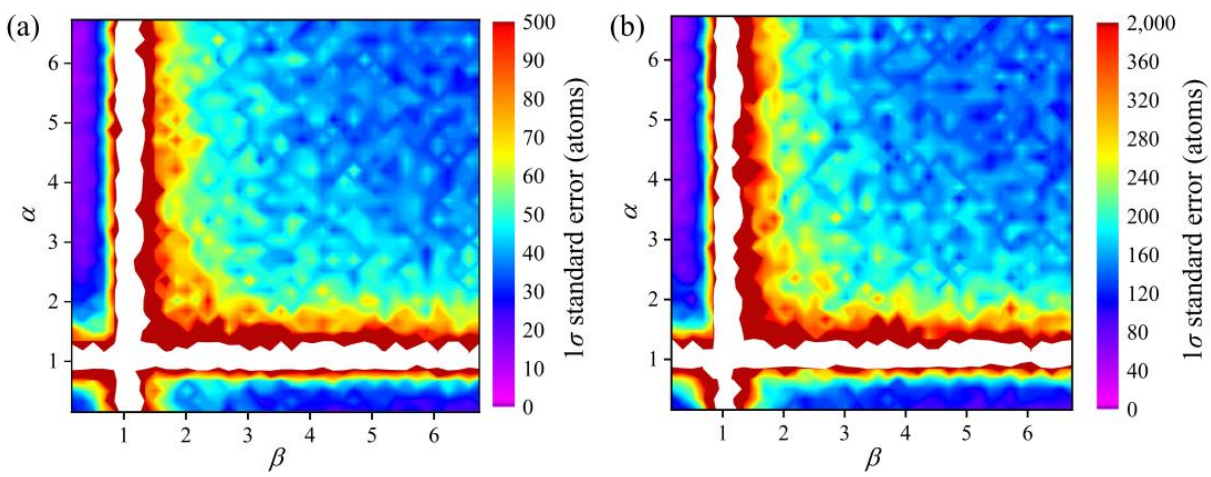

Figure 3. Numerical results of estimated uncertainties at different modulation parameters of α and β. (**a**) The standard deviation of 50 independent simulations at N_0 = 500. (**b**) The case of N_0 = 2000.

We also found that the maximum difference in estimated uncertainty within the ranges of α = 0.1~0.44 and β = 1.97~6.73 is below 4% at the current total simulated time of 6.7 h.

Therefore, we choose the parameters of α = 3.84 and β = 0.27 to numerically simulate the measurements of N_0 using our approach. Figure 4 demonstrates good agreement between numerical and theoretical results, as N_0 exceeds approximately 200. However, it should be noted that larger uncertainties are observed when N_0 is lower than 200, due to larger noise and reduced stability. The larger noise can correspond to stronger excitation fraction fluctuation, which may cause deviations in the half-height points of the Rabi spectrum more frequently. Although the frequency–sensitivity slope S_0 is not constant for the Rabi spectrum, we use a constant S_0 to infer N_0, leading to deviations for small N_0.

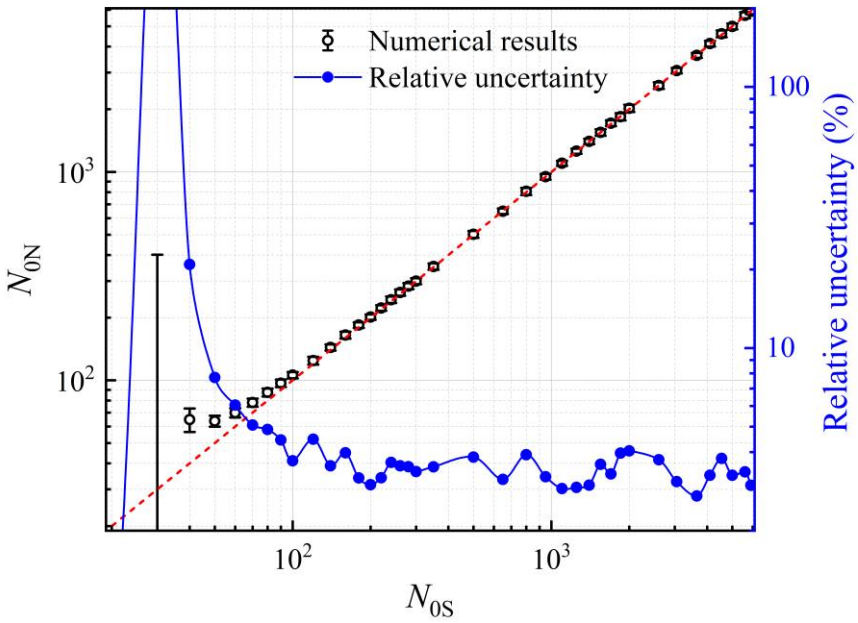

Figure 4. Numerical results of the determined atom number as a function of set value. Points are the results of single simulation, and the relative uncertainties are calculated by dividing error bars (the standard deviation of 50 numerical simulations) by corresponding set values. The dashed line indicates the theoretical values. As the atom number is smaller than 40, strong excitation fraction fluctuation leads to lock-lose, indicating the importance of maintaining a sufficiently high atom number to ensure stable and accurate measurements.

We verify our inference by conducting a comparison of N_0 simulated results using the Rabi and triangular spectra (shown in Figure 5), respectively. The values of S_0 remain unaffected by the frequency detuning on both the left and right sides in the case of a triangular spectrum. As a result, the stability calculation utilizing Equation (1) will not be influenced by fluctuations in the excitation fraction. Figure 4 demonstrates good agreement between theory and numerical result as the triangular spectrum is used, which is the powerful evidence of our hypothesis. Nevertheless, to achieve the triangular spectrum is challenging, this phenomenon suggests that our method can effectively work when N_0 exceeds about 200.

Exploring the relationship between total time consumption and estimated uncertainty using our approach presents an intriguing avenue for further study, given their crucial role in experiments. Figure 6 shows the relationship between relative uncertainty and total simulated time. It is evident that as the time increases, the uncertainties decrease following a slope of -0.5. This observation aligns with the fact that clock-comparison instability also decreases at the same slope of -0.5 with increasing averaging time. Through linear regression analysis, we determined that achieving a 1% uncertainty (one order of smaller than the typical uncertainty of absorption imaging [15–17]), requires a simulated time of approximately 20 h.

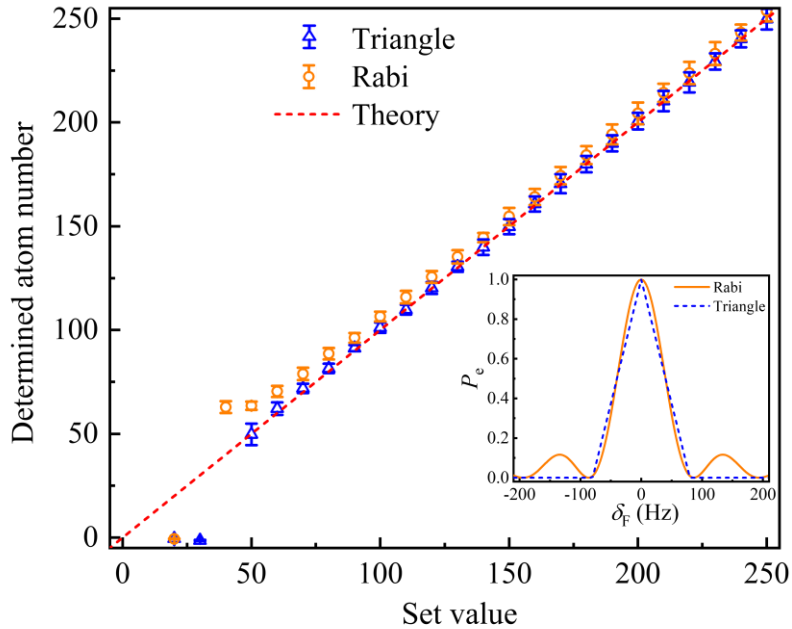

Figure 5. Numerical results of the determined atom number as a function of set value using the Rabi spectrum (circles) and triangular spectrum (triangles), respectively. Points are the results of single simulation, and the error bars indicate the standard deviation of 50 numerical simulations. The dashed line indicates the theoretical values. The inset shows the spectra of Rabi (solid line) and triangular spectrum (dotted line), respectively, wherein δ_F denotes frequency detuning and P_e represents excitation fraction.

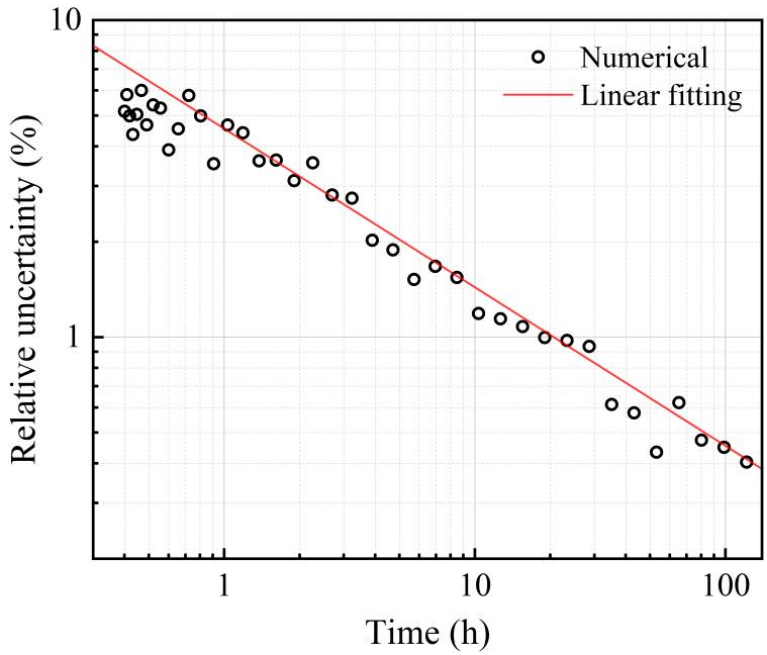

Figure 6. Relative uncertainty of the atom number measurement as a function of time consumption. The relative uncertainty is obtained by dividing the standard deviation of 50 numerical simulations by the atom number set at 2000. The red solid lines indicate the linear fitting with a fixed slope of −0.5.

In the real world, the number of atoms trapped in the lattice may vary from shot-to-shot clock cycles, making it important to study the relationship between the fluctuation amplitude of atom number and estimated uncertainty using our method. Both factors are critical in experiments. To induce atom number fluctuations, we added discrete random

integers to the set value of N_0 in every clock cycle, where the added noise followed a normal distribution N~(2000, 2000σ_f), where σ_f represents the fractional fluctuation of the atom number and can be ranged from 0 to 1. Figure 7a shows the atom number as a function of simulated time, while Figure 7b presents the numerical results of the extracted averaging atom number and corresponding relative uncertainty as a function of σ_f. Surprisingly, we found that the estimated uncertainty is almost independent of σ_f when the value of σ_f is smaller than approximately 14%. However, for larger values of σ_f, the estimated uncertainty rapidly increases, and the determined atom number deviates from the theoretical value of 2000. Figure 7b indicates that our method is effective, as long as the standard deviation of atom number fluctuation is controlled below 0.14 times the averaging atom number.

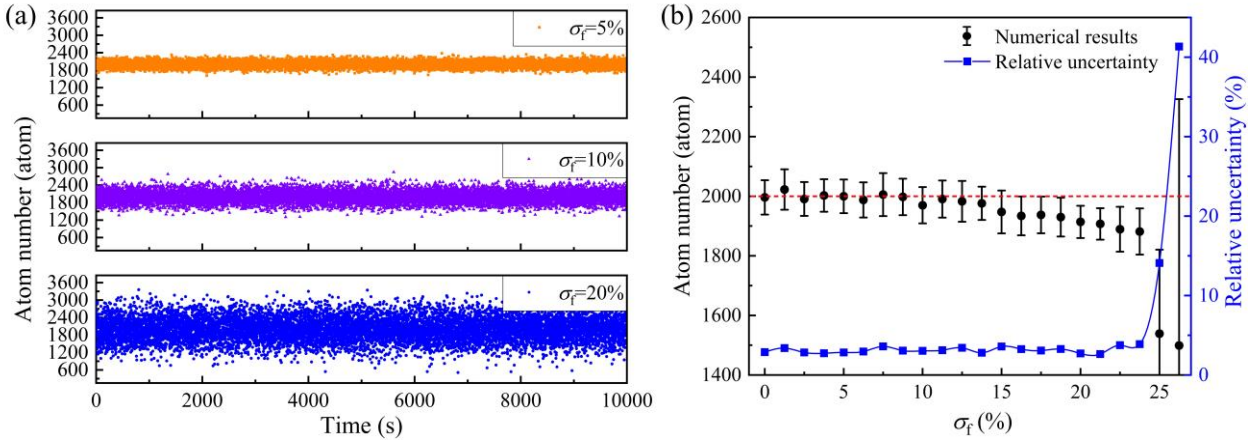

Figure 7. The atom number fluctuation and estimated uncertainty as a function of σ_f. (**a**) The fluctuation of atom number at σ_f = 5%, 10% and 20%, respectively. (**b**) Measurements of the atom number (averaging value of 50 simulations) and corresponding relative uncertainty (the standard deviation of 50 simulations) as a function of σ_f. The dashed line shows the set averaging number of atom of 2000.

4. Conclusions

In conclusion, our proposed method provides a valuable tool for accurately measuring the atom number in an OLC system where clock stability is limited by quantum projection noise, photon shot noise, and technical noise. The numerical results indicate that our approach can achieve an estimated uncertainty below 4% for atom numbers ranging from 50 to 6000 (the maximum setting value in this study). Furthermore, this level of uncertainty is achieved with a total simulated time of 6.7 h. It is important to note that by increasing the simulated time, it is possible to further reduce the uncertainty even more. We also investigated how the fluctuation of atom number affects the measurement results. The numerical results indicate that the standard deviation of atom number fluctuation should be controlled to be below 0.14 times the average atom number. Ensuring a stable atom number over an extended period is crucial in our proposed method. This can be achieved by controlling the atom number during the first stage of cooling and trapping, for example, by providing feedback on the duration of the Zeeman slower or the two-dimensional collimation light [29]. This work can advance research in many-body interaction [13,14,19], nondestructive detection [30], and entanglement of atoms [31], as the precise measurement of atom number enables more precise control and manipulation of atomic systems.

Author Contributions: Writing—original draft preparation, G.Z. and F.G.; software, G.Z., F.G. and X.L.; writing—review and editing, X.L. and H.C.; supervision, H.C. All authors have read and agreed to the published version of the manuscript.

Funding: This work is supported by the National Natural Science Foundation of China (Grant No. 12203057), and the Strategic Priority Research Program of the Chinese Academy of Sciences (Grant No. XDB35010202).

Data Availability Statement: The data presented in this study are available on request from the corresponding author.

Conflicts of Interest: The authors declare no conflicts of interest.

References

1. Bothwell, T.; Kedar, D.; Oelker, E.; Robinson, J.M.; Bromley, S.L.; Tew, W.L.; Ye, J.; Kennedy, C.J. JILA SrI optical lattice clock with uncertainty of 2.0×10^{-18}. *Metrologia* **2019**, *56*, 065004. [CrossRef]
2. McGrew, W.F.; Zhang, X.R.; Fasano, J.S.; Schäffer, A.; Beloy, K.; Nicolodi, D.; Brown, R.C.; Hinkley, N.; Milani, G.; Schioppo, M.; et al. Atomic clock performance enabling geodesy below the centimetre level. *Nature* **2018**, *564*, 87. [CrossRef] [PubMed]
3. Brewer, S.M.; Chen, J.S.; Hankin, A.M.; Clements, E.R.; Chou, C.W.; Wineland, D.J.; Hume, D.B.; Leibrandt, D.R. $^{27}Al^{+}$ quantum-logic clock with a systematic uncertainty below 10^{-18}. *Phys. Rev. Lett.* **2019**, *123*, 033201. [CrossRef]
4. Gross, C.; Bloch, I. Quantum simulations with ultracold atoms in optical lattices. *Science* **2017**, *357*, 995. [CrossRef] [PubMed]
5. Nunn, J.; Dorner, U.; Michelberger, P.K.; Lee, C.; Langford, N.K.; Walmsley, I.A.; Jaksch, D. Quantum memory in an optical lattice. *Phys. Rev. A* **2010**, *82*, 022327. [CrossRef]
6. Daley, A.J.; Boyd, M.M.; Ye, J.; Zoller, P. Quantum computing with Alkaline-earth-metal atoms. *Phys. Rev. Lett.* **2008**, *101*, 170504. [CrossRef] [PubMed]
7. Yin, M.J.; Lu, X.T.; Li, T.; Xia, J.J.; Wang, T.; Zhang, X.F.; Chang, H. Floquet engineering Hz-level Rabi spectra in shallow optical lattice clock. *Phys. Rev. Lett.* **2022**, *128*, 073603. [CrossRef] [PubMed]
8. Lu, X.T.; Wang, T.; Li, T.; Zhou, C.H.; Yin, M.J.; Wang, Y.B.; Zhang, X.F.; Chang, H. Doubly modulated optical lattice clock: Interference and topology. *Phys. Rev. Lett.* **2021**, *127*, 033601. [CrossRef]
9. Schwarz, R.; Dörscher, S.; Al-Masoudi, A.; Benkler, E.; Legero, T.; Sterr, U.; Weyers, S.; Rahm, J.; Lipphardt, B.; Lisdat, C. Long term measurement of the ^{87}Sr clock frequency at the limit of primary Cs clocks. *Phys. Rev. Res.* **2020**, *2*, 033242. [CrossRef]
10. Takamoto, M.; Ushijima, I.; Ohmae, N.; Yahagi, T.; Kokado, K.; Shinkai, H.; Katori, H. Test of general relativity by a pair of transportable optical lattice clocks. *Nat. Photon.* **2020**, *14*, 411. [CrossRef]
11. Miyake, H.; Pisenti, N.C.; Elgee, P.K.; Sitaram, A.; Campbell, G.K. Isotope-shift spectroscopy of the $^1S_0 \rightarrow {}^3P_1$ and $^1S_0 \rightarrow {}^3P_0$ transitions in strontium. *Phys. Rev. Res.* **2019**, *1*, 033113. [CrossRef]
12. Kennedy, C.J.; Oelker, E.J.; Robinson, M.; Bothwell, T.; Kedar, D.; Milner, W.R.; Marti, G.E.; Derevianko, A.; Ye, J. Precision metrology meets cosmology: Improved constraints on ultralight dark matter from atom-cavity frequency comparisons. *Phys. Rev. Lett.* **2020**, *125*, 201302. [CrossRef]
13. Zhou, Y.H.; Zhang, X.F.; Wang, T. Density shift of optical lattice clocks via the multiband sampling exact diagonalization method. *Phys. Rev. A* **2023**, *108*, 033304. [CrossRef]
14. Rey, A.M.; Gorshkov, V.C.A.; Kraus, V.M.; Martin, J.; Bishof, M.; Swallows, M.D.; Zhang, X.; Benko, C.; Ye, J.; Lemke, N.D.; et al. Probing many-body interactions in an optical lattice clock. *Ann. Phys.* **2014**, *340*, 311. [CrossRef]
15. Gregor, O.K.; Melina, P.; Gustav, W.; Mark, B.; Olivier, M.; Wolf, K. Atom number calibration in absorption imaging at very small atom numbers. *Cent. Eur. J. Phys.* **2012**, *10*, 1054.
16. Reinaudi, G.; Lahaye, T.; Wang, Z.; Guery-Odelin, D. Strong saturation absorption imaging of dense clouds of ultracold atoms. *Opt. Lett.* **2007**, *32*, 3143. [CrossRef]
17. Hueck, K.; Luick, N.; Sobirey, L.; Siegl, J.; Lompe, T.; Moritz, H.; Clark, L.W.; Chin, C. Calibrating high intensity absorption imaging of ultracold atoms. *Opt. Express* **2017**, *25*, 8670. [CrossRef]
18. Bothwell, T.; Kennedy, C.J.; Aeppli, A.; Robinson, J.M.; Oelker, E.; Staron, A.; Ye, J. Resolving the gravitational redshift across a millimetre-scale atomic sample. *Nature* **2022**, *602*, 420. [CrossRef]
19. Aeppli, A.; Chu, A.J.; Bothwell, T.; Kennedy, C.J.; Kedar, D.; He, P.; Rey, A.M.; Ye, J. Hamiltonian engineering of spin-orbit-coupled fermions in a Wannier-Stark optical lattice clock. *Sci. Adv.* **2022**, *8*, eadc9242. [CrossRef]
20. Santarelli, G.; Laurent, P.; Lemonde, P.; Clairon, A.; Mann, A.G.; Chang, S.; Luiten, A.N.; Salomon, C. Quantum projection noise in an atomic fountain: A high stability cesium frequency standard. *Phys. Rev. Lett.* **1999**, *82*, 4619. [CrossRef]
21. Al-Masoudi, A.; Dörscher, S.; Häfner, S.; Sterr, U.; Lisdat, C. Noise and instability of an optical lattice clock. *Phys. Rev. A* **2015**, *92*, 063814. [CrossRef]
22. Lu, X.T.; Xia, J.J.; Lu, B.Q.; Wang, Y.B.; Wang, T.; Chang, H. Determining the atom number from detection noise in a one-dimensional optical lattice clock. *Appl. Phys. Lett.* **2022**, *120*, 151104. [CrossRef]
23. Takamoto, M.; Takano, T.; Katori, H. Frequency comparison of optical lattice clocks beyond the Dick limit. *Nat. Photon.* **2011**, *5*, 288. [CrossRef]
24. Lu, X.T.; Zhou, C.H.; Li, T.; Wang, Y.B.; Chang, H. Synchronous frequency comparison beyond the Dick limit based on dual-excitation spectrum in an optical lattice clock. *Appl. Phys. Lett.* **2020**, *117*, 231101. [CrossRef]
25. Campbell, S.L.; Hutson, R.B.; Marti, G.E.; Goban, A.; Darkwah Oppong, N.; McNally, R.L.; Sonderhouse, L.; Robinson, J.M.; Zhang, W.; Bloom, B.J.; et al. A Fermi-degenerate three-dimensional optical lattice clock. *Science* **2017**, *358*, 90. [CrossRef]

26. Lemonde, P.; Laurent, P.; Santarelli, G.; Abgrall, M.; Sortais, Y.; Bize, S.; Nicolas, C.; Zhang, S.; Clairon, A.; Dimarcq, N.; et al. *Frequency Measurement and Control: Advanced Techniques and Future Trends*; Springer: Berlin/Heidelberg, Germany, 2001; Volume 79, pp. 131–153.
27. Dick, G.J. Local oscillator induced instabilities in trapped ion frequency standards. In Proceedings of the 19th Annual Precise Time and Time Interval Meeting, Redendo Beach, CA, USA, 1–3 December 1987; pp. 133–147.
28. Nicholson, T.L.; Martin, M.J.; Williams, J.R.; Bloom, B.J.; Bishof, M.M.; Swallows, D.; Campbell, S.L.; Ye, J. Comparison of two independent Sr optical clocks with 1×10^{-17} stability at 10^3 s. *Phys. Rev. Lett.* **2012**, *109*, 230801. [CrossRef]
29. Wang, Y.B.; Yin, M.J.; Ren, J.; Xu, Q.F.; Lu, B.Q.; Han, J.X.; Guo, Y.; Chang, H. Strontium optical lattice clock at the National Time Service Center. *Chin. Phys. B* **2018**, *27*, 023701. [CrossRef]
30. Orenes, D.B.; Sewell, R.J.; Lodewyck, J.; Mitchell, M.W. Improving short-term stability in optical lattice clocks by quantum nondemolition measurement. *Phys. Rev. Lett.* **2020**, *128*, 153201. [CrossRef]
31. Pedrozo-Peñafie, E.; Colombo, S.; Shu, C.; Adiyatullin, A.F.; Li, Z.Y.; Mendez, E.; Braverman, B.; Kawasaki, A.; Akamatsu, D.; Xiao, Y.H.; et al. Entanglement on an optical atomic-clock transition. *Nature* **2020**, *588*, 414. [CrossRef]